Intercontinental transport of ozone and its precursors in a 3-D global CTM

Oliver Wild, and Hajime Akimoto
Frontier Research System for Global Change, Yokohama, Japan

Abstract

The coupling of chemistry with atmospheric transport processes provides a mechanism for local and regional pollution from heavily populated continental regions to influence tropospheric composition at hemispheric and global scales. In this study we use the FRSGC/UCI 3-D chemical transport model to quantify the impact of ozone precursors from anthropogenic sources in the United States, Europe and East Asia on regional and global ozone budgets and to identify the key controlling processes. We find that the East Asian region has the greatest potential to affect tropospheric ozone due principally to efficient vertical transport, but that Europe experiences the greatest intercontinental effects due to rapid, short-distance transport from North America. In addition to significant boundary layer ozone production in each region, we find that 25–40% of the total net regional production occurs above 730 hPa in the free troposphere, and that on a hemispheric scale 70–85% of ozone from anthropogenic sources in the upper troposphere, above 400 hPa, is due to *in-situ* chemistry rather than direct vertical transport. Increased surface ozone concentrations over remote continents are largest in spring and autumn at northern mid-latitudes; while this seasonality is driven by horizontal transport in the free troposphere followed by subsidence, boundary layer and upper tropospheric chemical production make a substantial contribution. Although the effects are greatest in periodic episodes when meteorological conditions are favourable, there is significant enhancement in background ozone concentrations. We suggest that increasing emissions will significantly impact the oxidizing capacity of the troposphere by leading to greater polarization between ozone production and destruction environments.

1. Introduction

The oxidizing capacity of the troposphere depends strongly on ozone as a source of the principal oxidizing agent, the hydroxyl radical, OH. While flux from the stratosphere is a significant source of ozone in the troposphere, it is clear that chemical formation from precursors of anthropogenic origin also plays an important role [*Chameides and Walker,* 1973]. Comparison of recent ozone measurements with those from the end of last century [*Volz and Kley,* 1988] show significant increases which may be largely attributable to increases in anthropogenic emissions of precursors. However, production of ozone from these sources and transport to the global atmosphere has generally been considered in a regional context [e.g., *Jacob et al.,* 1993; *Kotamarthi and Carmichael,* 1990]. The importance of regional ozone pollution in North America, Europe and Eastern Asia has been highlighted by *Chameides et al.* [1994], who termed these regions with both intense urban-industrial and agricultural activities 'metro-agro-plexes', and who drew attention to the impacts on crop growth as well as on urban air quality. However, these three regions lie in a similar latitude band in the Northern Hemisphere, and their pollution problems may therefore be readily coupled by atmospheric transport processes. While the lifetime of the major oxidant precursors, NO_x (NO + NO_2) and reactive hydrocarbons may only be 1–2 days in the lower troposphere, the ozone they form has a lifetime of days to months. Typical transport times between continents are 5–10 days, and there is therefore significant potential for one continental region to affect another, suggesting that regional pollution should be considered in a global context.

Intercontinental transport is observed most clearly in the transport of aerosol over the ocean, for example desert dust [e.g., *Duce et al.,* 1980] and soot from large fires [*Bodhaine et al.,* 1992]. While similar processes affect gas-phase pollutants, these episodes are more difficult to detect, and are not as easily attributable to long-range transport due to significant and often highly variable 'background' concentrations and to the wide variety of potential sources. However, measurements from the STARE campaign [*Andreae et al.,* 1996] identified the role of biomass burning over Africa on episodes of high ozone concentrations over the tropical Atlantic. Similarly, aircraft and surface measurement campaigns over the mid-latitude North Atlantic [*Fehsenfeld et al.,* 1996] and Pacific Oceans [*Hoell et al.,* 1997] have followed the evolution and export of continental pollution plumes, while observations over Europe [*Stohl and Trickl*, 1999] and the west coast of the U.S. [*Jaffe et al.,* 1999] have detected unusually high concentrations of oxidants and their precursors in air masses that can be traced back to very distant source regions using trajectory techniques. Recent studies using 3-D global chemical transport models (CTM) have demonstrated the potential of intercontinental transport to affect oxidant concentrations over the Atlantic [*Atherton et al.,* 1996] and Pacific Oceans [*Berntsen et al.,* 1999], and have started to address the implications of increasing global emissions on regional ozone concentrations [*Jacob et al.,* 1999; *Collins et al.,* 2000].

This paper addresses the impacts of long-range transport on the regional ozone budget over the main Northern Hemisphere population regions and on the oxidising capacity of the troposphere on a global scale. We focus on the extent to which precursor emissions from each region affect ozone concentrations over each other region, and on how these influences vary through the year. We quantify the relative importance of chemistry and transport in controlling the export of oxidants and precursors, and how the balance between these processes changes during the year. While chemical processes control oxidant formation in the polluted continental boundary layer, ozone production in the free troposphere following vertical transport of precursors by rapid mechanisms such as convection [*Pickering et al.,* 1990] or slower, frontal lifting [*Bethan et al.,* 1998] supplements the direct transport of oxidants from the boundary layer. The balance between these processes is driven by local and regional meteorology, and differs substantially from season to season and from one region to another. To quantify these effects, and to extend previous regional studies of oxidant budgets [*Jacob et al.,* 1993; *Liang et al.,* 1998], we apply a global model to allow direct comparison of the main emission regions and to investigate the coupling between them.

In section two, we describe the FRSGC/UCI GISS II′ CTM used in the current studies, and demonstrate its strengths and weaknesses in simulating the budgets of oxidants in the present-day atmosphere. In section three, we present oxidant budgets for the three major northern hemisphere population regions, and compare with previous measurement and modelling estimates. We then describe perturbation studies varying precursor emissions for selected regions in section four, determining the impacts on oxidant budgets at regional and global scales, and highlighting the effects of each region on ozone concentrations over the

other regions. We conclude by highlighting the mechanisms controlling these impacts, demonstrating the different balance between them over the different regions, and by considering the implications of recent increases in emissions over East Asia.

2. Model Overview

The tropospheric modelling studies described in this paper make use of the FRSGC/UCI CTM, the latest in a generation of models developed at the University of California, Irvine, based on meteorological fields from the Goddard Institute of Space Sciences (GISS) GCM. The model is described in detail in *Wild and Prather* [2000], and only a brief summary will be provided here. It uses 3-hour averaged fields with a horizontal resolution of 4° latitude × 5° longitude, and a vertical resolution of nine levels from the surface to 10 hPa, with six to eight levels in the troposphere. Advection is calculated using the Prather scheme conserving second-order moments [*Prather,* 1986]. Entraining and non-entraining convective mass fluxes are supplied as 3-hour averages from the meteorological fields. The height of the boundary layer is diagnosed from the fields, and mixing is calculated every CTM time step using the scheme of *Louis* [1979].

The model includes a detailed tropospheric chemical scheme using the ASAD modular chemistry package [*Carver et al.,* 1997], with a fast implicit solver for the chemical equations. The chemical module includes an explicit treatment of inorganic $HO_x/O_x/NO_x$ chemistry and methane oxidation, and a lumped 'family' treatment of hydrocarbon oxidation for the representative species butane, propene, xylene and isoprene. Photolysis rates are calculated using the Fast-J photolysis scheme [*Wild et al.,* 2000], which has an on-line treatment of molecular and aerosol absorption and scattering, allowing the full variability of photolysis rates to be captured on short time scales as the cloud fields vary.

Emissions of trace species are taken from the EDGAR v.2.0 database for 1990 [*Olivier et al.,* 1996], supplemented with soil emissions of NO [*Yienger and Levy,* 1995] and emissions of isoprene from vegetation [*Guenther et al.*, 1995] reduced to 220 Tg(C)/yr consistent with *Brasseur et al.* [1998]. A source of NO from lightning, 5 Tg(N)/yr, is included based on the parameterization of *Price and Rind* [1992]. The choice of emission datasets has been assessed by sensitivity studies using the GEIA emissions datasets for 1985 (see *Wild and Prather* [2000] and references therein); although there are some differences in regional budgets, the variations are not substantially different, and do not affect the conclusions of this study. Dry deposition is treated using a 'resistances-in-series' scheme based on that of *Jacob et al.* [1992], using surface meteorological properties, vegetation type and species solubility. Wet deposition is parameterised by loss of soluble species in wet convective updrafts, and by removal by below-cloud scavenging when precipitation is diagnosed from the meteorological fields. A dynamical tropopause is diagnosed online using the 120 ppbv isopleth of an inert, O_3-like tracer 'Synoz' [*McLinden et al.,* 2000] which is emitted at 475 Tg/yr in the stratosphere, removed at the surface, and has previously been run to steady-state. This tracer is allowed to define the flux of O_3 and NO_y from the stratosphere; for other species the effects of stratospheric chemistry are simulated by providing first-order removal rates. A marker of stratospheric ozone, initialised like Synoz and removed by chemical loss in the troposphere, has been added to allow the stratospheric influence on ozone to be diagnosed.

For the present studies we have reduced the model resolution to $8° \times 10°$ by combining variables at $4° \times 5°$ to ease the computation burden without significant loss of accuracy. Use of the second-order moment scheme, which allows a degree of localization of tracer mass within grid boxes, minimises the impacts of this degradation, and tracer distributions show only small differences except in boundary regions. The ability of the model to simulate the tropospheric distribution of trace gases has been evaluated by comparing with observations from measurement campaigns, ozonesonde profiles and individual measurement stations. Comparisons for O_3, CO, NO_y and PAN are presented in *Wild and Prather* [2000]; further evaluation has been made using by comparing with aircraft measurements from recent NASA GTE campaigns.

Figure 1 shows the monthly variations in ozone at three altitudes compared with ozonesonde profiles from *Logan* [1999]. In general, the magnitudes and seasonal variations are reproduced relatively well, but the figure illustrates a number of limitations in the model simulation. The location of the exchange of air between the stratosphere and the troposphere is not well represented in the GISS II′ meteorological fields [*Rind et al.,* 1999], and as a consequence ozone concentrations are overestimated in high latitude regions in Spring in the chemical simulations, and this can be seen at 250 hPa as far south as Boulder. However, these effects are controlled by use of the 'Synoz' tracer

to define the total stratospheric input of O_3 and NO_y, and are minimized in the present studies by the focus on anthropogenicly-driven perturbations. Ozone concentrations in the most polluted parts of the continental boundary layer may be slightly overestimated, as seen at Hohenpeissenberg, due to the lack of a subgrid scale treatment of the high spatial variability in emissions in these polluted regions, which may lead to overestimation of regional ozone production due to non-linearities in ozone formation [*Jacob et al.,* 1993; *Liang and Jacobson,* 2000]. The summertime dip in mid-tropospheric O_3 in the model over Sapporo, clearly seen in the ozonesondes at Tateno and Kagoshima in southern and central Japan, is due to greater influence from air over the Tropical Pacific during this season. However, this is not observed as far north as Sapporo, and illustrates the limitations of the coarse model resolution used. However, the distributions of many short-lived species have been compared with measurements over Hokkaido [H. Tanimoto, personal communication], and are relatively well reproduced, both in absolute magnitude and in the horizontal, vertical and temporal variation.

The global ozone budget is similar to that derived in other studies; after three years of spin-up, allowing cross-tropopause and inter-hemispheric transport to fully redistribute the initial tracer concentrations, stratospheric injection accounts for 475 Tg of tropospheric ozone annually, chemical production for 230 Tg (production 3680 Tg, loss 3450 Tg), and 704 Tg is deposited at the surface. Figure 2 shows the seasonal variation in the three major budget terms by hemisphere, and demonstrates the dominance of the northern hemisphere in controlling the total ozone budget. Input from the stratosphere peaks in winter in the Northern Hemisphere and in spring in the Southern Hemisphere, whereas chemical production and deposition peak in Northern Hemisphere summer, reflecting the importance of the Northern Hemispheric sources of precursors. Most of the chemical production occurs in the lowest 2 km above the surface, where emissions of precursors occur, or in the upper troposphere, where they are lifted to by convection or introduced by lightning or aircraft. In the lower mid-troposphere, chemical destruction dominates, reflecting losses to photolysis and formation of OH radicals. Deposition fluxes follow the ozone concentrations, being greatest in boreal summer when chemical production dominates and in austral spring when stratospheric injection and production from biomass burning emissions are greatest. The hemispheric mean values in this figure do not emphasize the large longitudinal gradients in O_3 production and loss near the surface; the marine boundary layer shows consistent, large net loss, whereas the continental boundary layer with industrial NO_x emissions shows an overwhelming net production.

3. Continental Budgets

The chemical budgets of ozone and NO_x have been derived for the major northern hemisphere population regions from a standard control run of the CTM, and form the basis with which subsequent runs are compared. The regions selected, shown in Figure 3, cover the major emission regions of the United States, Europe and East Asia, and are similar in area. Between them, the regions account for more than 65% of the annual surface fossil fuel sources of NO_x from the EDGAR inventory. Mean annual budgets are calculated for the boundary layer, defined as the lowest three model levels, up to $\sigma = 0.73$ (typically about 2.2 km), and for the troposphere up to $\sigma = 0.15$ (about 13 km), and are shown in Table 1. The net O_3 production includes chemical formation from precursors from all sources; the net export is the difference between transport of chemically-produced O_3 out of the region and transport of free-tropospheric O_3 in. Each region is a net exporter of O_3; in addition, about 20% of emitted nitrogen is exported from the boundary layer as NO_x or the reservoir species peroxyacetylnitrate, PAN, most of which is lifted into the free troposphere and leads to further *in-situ* O_3 production. Total net production over each region between the surface and 150 hPa (about 13 km) is indicated at the bottom of the table; while the free troposphere is a smaller source than the boundary layer, the additional 20–25 Tg/yr production, 25–40% of the total regional O_3 production, makes a substantial contribution to the total exports from each region.

The annual export of ozone from the U.S. boundary layer (11 Tg/yr) is similar to that of *Liang et al.* [1998] (6 Tg/yr), although the variation in chemical ozone tendency through the depth of the lower troposphere and the confinement of deposition to the surface make this value rather sensitive to the definition of the boundary layer. Net ozone import occurs in the winter and spring, when chemical formation is reduced and stratospheric input larger, while net export occurs in the summer and autumn, when chemical formation is more rapid and the influence of the stratosphere reduced. Net boundary layer pro-

duction, at 61 Tg/yr, is very similar to the 63 Tg/yr derived by *Liang et al.* [1998]. The ozone production efficiency, defined here as the net number of molecules of O_3 produced per molecule of NO_x oxidised [*Lin et al.,* 1988], peaks at 4.8 in the summer, somewhat less than the 6.3 derived by *Jacob et al.* [1993]; in the winter it drops to 1.1. The net summer-time export of O_3 from the U.S. region, 52 Tg/yr, is somewhat less than the 75 Tg/yr found by *Jacob et al.* [1993], but does not account for the influx and removal of O_3 from tropospheric sources outside the region. The export of NO_x and PAN is 1.4 Tg(N), the same as that derived by *Liang et al.* [1998], and constitutes 18% of the annual emissions; peaking at 27% in winter, this fraction drops to 13% in summertime, similar to the 12.5% derived by *Horowitz et al.* [1998].

Export of ozone from the European boundary layer is smaller in magnitude due to slightly lower emissions and lower production efficiencies; slower formation rates and significant wintertime titration in Northern European industrial regions, which have high NO_x emission densities, lead to reduced production and export. The ozone production efficiency reaches only 3.8 in the summer, and is close to zero in the winter, indicating that titration over Northern Europe is almost equal to production over Southern Europe. A slightly greater fraction of NO_x emissions, 21%, is exported from the boundary layer than for North America, and significant additional ozone production occurs in the free troposphere over the region, about 20 Tg/yr, similar to that over the U.S.

Net production of ozone in the boundary layer over East Asia is less than that for North America, but greater than for Europe. The ozone production efficiency is higher, peaking at 6.4 in the summer, reflecting lower NO_x emission intensities and more southerly latitudes. Surface deposition is less than for the U.S., due in part to faster vertical transport out of the boundary layer, and this greater venting also leads to greater net production above the boundary layer, 25.6 Tg/yr compared to 21.0 Tg/yr. Consequently, net O_3 export from the region is also larger. *Mauzerall et al.* [2000] make an upper estimate of O_3 export from East Asia of 58 Tg/yr; our estimate of 40 Tg/yr is somewhat lower, but does not account for the influx and removal of O_3 from stratospheric sources (13 Tg/yr), which brings the figures into good agreement.

4. Anthropogenic Emissions

To determine the effects of anthropogenic emissions on regional and global ozone budgets, we increase the emissions of NO_x, CO and NMHC from surface fossil fuel sources by 10% for each region in turn. This perturbation was chosen to be small enough to avoid significant non-linear chemical influences on O_3 formation, but large enough to produce a measurable global response. In addition, it provides a reasonably realistic short-term scenario for the East Asian region, where NO_x emissions are currently thought to be increasing at 4–5% a year [*van Aardenne et al.,* 1999; *Streets and Waldhoff,* 2000]. For this region, emissions were increased west of 130°E, thereby focusing on the developing nations of the region, principally China, and excluding Japan. However, the ratio of emissions has been held constant to explore the current chemical environment, and hence the results may not be truly representative of future trends.

In each case, the CTM was initialised with chemical fields for July from an earlier 2-year run of the model, and run for 18 months, discarding the first 6-month period. In addition to the standard chemical species, an inert tracer, '$i$$NO_x$', was released globally at the same rate as fossil fuel NO_x emissions, and provided with a first-order removal time of 10 days, to assess the effects of transport independent of chemical processes. For each scenario, the impacts of the additional emissions on oxidant budgets over each region were assessed for each month by taking the difference between the budget terms and those in the control run. We first look at the annual, global changes, and then focus on seasonal variations and regional differences and on the mechanisms which control them.

4.1. Regional Budgets

Over each region, increased emissions lead to greater net chemical O_3 production over the global troposphere, see Table 2. In each case, about 95% of the additional O_3 is deposited to the surface; the rest contributes to increased atmospheric concentrations. The proportion is slightly less for East Asia, where vertical transport leads to a greater interaction with the model stratosphere; the length of the runs is insufficient to allow redistribution throughout the stratosphere and hence to establish a steady-state impact on the global burden.

Additional net O_3 production in the regional boundary layer for U.S. and East Asian emissions is greater

than the increase in global net production, indicating that the global troposphere outside the continental boundary layer is a net sink of pollution O_3 on an annual basis; over Europe, where wintertime titration significantly reduces additional O_3 formation, 35% of the total net formation is outside the region. Additional formation over East Asia exceeds that over the U.S., despite lower precursor emissions, principally because of the lower emission intensities over the region, hence higher production efficiencies, and the relatively small contribution from wintertime titration. The ozone production efficiencies calculated from the additional formation are rather lower than those derived for each region in Table 1, reflecting the greatest absolute increases in emissions in areas which already have high emissions, and providing a weighting towards areas with low production efficiencies.

The fraction of pollution O_3 exported is fairly similar over each region, 66–77% of the additional net O_3 production. The proportion is largest for East Asia, where greater vertical transport leads to the shortest residence time, 2.6 days to transport and deposition on an annual basis, compared to 4.2 days for the U.S. and 5.7 days over Europe. The export fraction for the U.S. boundary layer, 66%, is similar to that found in previous studies; *Liang et al.* [1998] derive a value of 73%, and *Jacob et al.* [1993] a summertime value of 70%. We find that the June–August period accounts for about half of the annual exports from the region; while there is almost no export in winter, spring accounts for about 30% and autumn for about 20% of total exports.

Table 2 also shows the relative roles of chemistry and vertical transport in controlling O_3 from anthropogenic sources in the upper troposphere. Directly over each region, direct transport of O_3 and net chemical production from transported precursors make similar contributions to the additional O_3; for the U.S. and East Asia direct transport is slightly more important, while for Europe it is somewhat less important. However, on a global basis, additional *in-situ* production dominates, and direct transport only accounts for 14–30% of the upper tropospheric O_3 enhancement. Most of the additional O_3 production (64–73%) occurs beyond the boundaries of the regions, emphasising the faster transport and longer NO_x and O_3 lifetimes at these altitudes. As in the boundary layer, East Asia has the greatest impacts, with about 30% greater O_3 enhancements than for the U.S.; this highlights the critical role played by vertical transport processes in enhancing both direct transport and additional chemical production.

4.2. Global Influences

The spatial extent of the annual mean changes in O_3 and its chemical tendency are shown in Figures 4 and 5. The change in O_3 mixing ratio is greatest in the boundary layer over the emission region, but significant impacts are also seen in the upper troposphere to the extent that the peak zonal mean enhancements are seen at northern mid-latitudes. The meridional mean figures highlight the enhancements in O_3 above the polluted boundary layer and some way downwind of the region; in the case of East Asian emissions, vertical transport processes take O_3 and precursors sufficiently close to the tropopause that they interact with the model stratosphere. The extent to which additional O_3 is found downwind of source regions is evident from the column mean figures; that this occurs to the greatest degree in the mid and upper troposphere can be seen from the meridional means. Note the different latitudinal influences, as European emissions give the greatest enhancements over Polar regions, while East Asian emissions occur sufficiently far south to affect the Tropics, and consequently have a greater influence in the Southern Hemisphere.

The change in the chemical O_3 tendency, shown in Figure 5, highlights the regional effects clearly, and emphasizes the role of chemistry beyond the polluted boundary layer. While regional boundary layer production is enhanced, significant additional production occurs on a hemispheric scale at higher altitudes. The importance of vertical transport processes in enhancing upper tropospheric O_3 formation by lofting precursors is clear and accounts for much of the difference between regions; for Europe, where vertical transport plays a smaller role, enhancement of O_3 formation is restricted to the lower and mid troposphere, and the global extent is reduced. For East Asia, where O_3 and precursors are lifted highest, the large additional upper tropospheric production is partially offset by reduced production in the mid-troposphere over the emission region compared to the other scenarios. Increased O_3 destruction occurs principally in the mid-troposphere in outflow regions; while this is a maximum immediately east of each region, low-level southerly and southwesterly outflow leads to a net increase in destruction in the Northern Tropics. In the zonal and meridional mean figures, decreases in annual net O_3 production can be seen close to the surface for the Northeastern U.S. and Northwestern

Figures 4

Europe, where NO_x emissions are highest, providing evidence of wintertime ozone titration.

4.3. Intercontinental Transport

The extent to which the continental regions affect each other is illustrated in Figure 6, which shows the monthly variations in the O_3 perturbations at three altitudes over each region for each scenario. The mass-weighted mean mixing ratios are shown for each level, while the error bars give the spatial variance over each region. O_3 is most greatly enhanced in the boundary layer in the emission regions, as expected, with reduced perturbations at higher altitudes controlled by transport and chemistry. Downwind, the gradient is typically reversed, with higher values in the free troposphere than at the surface. All scenarios show summertime maxima in the emission region, and most show summertime minima outside the region, consistent with more rapid chemical formation and destruction and with variations in transport patterns bringing more air from southerly latitudes. Downwind regions see a spring maximum at the surface, and generally throughout the troposphere; most regions also see a secondary maximum in autumn. The spring maximum occurs at the same period that remote observation stations in Northern mid-latitude regions typically see maximum ozone concentrations [e.g., *Monks,* 2000], and underscores the contributions that tropospheric sources and transport make to this feature.

For East Asian emissions, upper tropospheric concentrations are enhanced to a greater extent than for the other scenarios, and strong enhancements are seen over the U.S., particularly in spring and autumn. This is also seen in the $i\mathrm{NO}_x$ tracer, shown in Figure 7, suggesting that it is principally due to more rapid, direct transport. This is supported by the relatively strong vertical gradient seen over the region. The spatial variability is large, reflecting the different sources and transport times over different parts of the U.S.; during the summer, when the westerly airflow is rather weaker, the perturbation is small. Interestingly, the magnitude of variations over Europe is similar to that over the U.S., but with a smaller variance due to the greater distance downwind and to the lower variability in flow patterns. O_3 enhancements at the surface are only about 10% less than over the U.S., 25% less in the mid-troposphere, and are about 10% more in the upper troposphere on an annual basis. This is partly due to the northward displacement of the principal transport pathway over North America in summertime, as the U.S. sees greater influence from more southerly air masses. However, the significant effects over Europe emphasise the role of upper tropospheric transport in enhancing surface O_3 on a hemispheric scale.

While the importance of transport in defining the seasonality is clear from the behaviour of the $i\mathrm{NO}_x$ tracer downwind of East Asia, the impacts for O_3 are strongly modulated by chemistry. The greater net summertime formation of ozone in the continental boundary layer contrasts with the lack of significant seasonality seen for the $i\mathrm{NO}_x$ tracer, and might therefore be expected to enhance the impact over the U.S. in summer; however the shorter chemical lifetime during transit and slower transport times offset this. In spring and autumn, when longer NO_x and NO_y lifetimes allow more to be carried up into the upper troposphere, the greater *in-situ* chemical production and shorter transport times ensure that these seasons remain dominant over the U.S. and Europe.

The impact of U.S. emissions on surface O_3 in Europe are the largest intercontinental effects seen here, and reflect the short transport times; air arriving in the mid-troposphere, below 400 hPa, sees the greatest enhancements. Surface enhancements average about 35% of those over the U.S. on an annual basis. The spring maximum at the surface is also seen in the $i\mathrm{NO}_x$ tracer, emphasising the importance of transport. However, the effects on East Asia are far smaller, principally because much of the flow follows a more northerly path, around the Tibetan Plateau; only the northern parts of China, Korea and Japan see greater influences, and the spatial variances are consequently large. The vertical gradient is relatively small, reflecting greater vertical mixing over the Eurasian continent, and the variations closely match those in the $i\mathrm{NO}_x$ tracer, suggesting that deposition of O_3 over Western and Central Asia makes up for additional O_3 formation during transport.

European emissions have the smallest downwind effects, due to less active vertical transport, despite greater extremes of boundary layer production and titration. Upper tropospheric O_3 is affected least of the three scenarios, but significant perturbations are still seen over both Asia and the U.S., particularly in Spring. It is notable that European emissions contribute as much to surface O_3 perturbations over the U.S. as emissions from Asia do, with a similar seasonality, but with much smaller effects in the upper troposphere, reflecting the different modes of transit. European emissions are found to have a greater ef-

fect on polar regions, and may thereby affect North America by a shorter route than mid-latitude transport around the globe. However, the polar regions are least well represented in the current model, and hence further analysis is required to support this result.

4.4. Mechanisms

The key mechanisms involved in export of pollution O_3 from the continental boundary layer are shown for the three study regions in Figure 8. Over each region O_3 formation is highest in summer, and hence net export is largest; however, the regions differ considerably in the relative importance of removal processes. Deposition and deep convection peak in summer, and are similar in magnitude except over the U.S., where deposition dominates. The principal difference between the regions arises from the contributions of non-convective vertical transport, typically slower transport associated with pressure systems and the passage of fronts. Over Europe, these processes have a very small impact on an annual mean basis; over East Asia, they exceed convection. Between February and May over East Asia about 65% of the vertical transport of O_3 is controlled by these processes; in summer, when high pressure systems trapping O_3 close to the surface are more common, horizontal advection dominates. Over Europe, where convection is rather weaker, large summertime high pressure regions are common, and horizontal advection in the boundary layer is the major export mechanism for much of the year. Note that the relative importance of these processes differs for other species. For short-lived species such as NO_x, where the vertical gradient is steep, the rapid exchange associated with convection dominates slower lifting processes and accounts for more than 90% of vertical export. This suggests that while convection accounts for only 40% of vertical export of O_3, chemical production above the boundary layer following these events will be rather greater than after slower lifting events.

To investigate the mechanisms controlling the fate of these oxidants on a global scale, we calculate monthly budgets and tendencies for O_3 over each region. In addition to the boundary layer, we define a mid-tropospheric layer (model levels 4 and 5, σ = 0.73–0.40, typically 2.2–6.4 km), and an upper tropospheric layer (levels 6 and 7, σ = 0.40–0.15, typically 6.4–13 km). We calculate fluxes for the same altitude bins for the global troposphere external to the region; the fluxes in these six domains are additive, and cover the whole of the troposphere from the surface to about 150 hPa. We consider the East Asian emissions perturbation to illustrate the mechanisms involved; we first focus on the 'iNO$_x$' tracer which has a fixed, first-order loss rate of 10 days, and then on O_3, where the chemical lifetime varies with season and region.

Figure 9 shows changes in the fluxes of the 'iNO$_x$' tracer over East Asia and over the rest of the globe due to 10% increased emissions over East Asia. In the boundary layer, the lifetime to vertical and horizontal transport is 3.3 days in January, but only 1.9 days in July, and hence the burden is about 60% greater in January than in July. Vertical transport into the free troposphere dominates exports for most of the year, but horizontal transport in the boundary layer is important from November to February; much of this occurs in the southernmost part of the region, where there is wintertime outflow towards India. The mid-troposphere sees greatest input from the boundary layer in March, when non-convective lofting reaches a maximum; the upper troposphere is more strongly controlled by convection, and input is greatest in summer, although temporary suppression of lofting provides a secondary minimum in July. Horizontal transport out of the emission region is maximum in the boundary layer in winter, peaks in March in the mid-troposphere, and shows broad spring and autumn maxima in the upper troposphere. The seasonality in the upper troposphere is reversed with respect to the boundary layer, emphasising the important role that vertical transport processes over emission regions play in controlling distributions downwind. Note that while the 'iNO$_x$' tracer is sensitive to transport time scales, the export patterns described here are representative of longer-lived pollutants such as CO, which shows a very similar seasonal variation in exports.

The budget of additional O_3, see Figure 9, shows similar patterns modulated by variations in chemical O_3 production. Net boundary layer O_3 formation peaks in July at about four times that in winter; the residence time of O_3 in the boundary layer is 2.3 days in July (8.4 days to deposition, 3.2 days to transport), and 4.0 days in January (43 days to deposition, 4.5 days to transport); the chemical lifetimes are 3.4 days and 6.4 days, respectively. Vertical transport dominates removal, and upper tropospheric enhancements are similar to those for the iNO$_x$ tracer, though the seasonality is stronger due to the greater summertime burden in the boundary layer. Vertical transport of short-lived species such as NO_x is dominated by deep

convection rather than by slower lifting processes; this leads to significant additional O_3 production in the upper troposphere which almost matches direct O_3 transport. In the mid troposphere, there is net production in spring, when the ratio of NO_x to O_3 in air lifted from the boundary layer is relatively large, but very little in summer, when boundary layer NO_x levels are lower and O_3 levels higher.

While horizontal transport of O_3 and NO_x out of the emission region occurs at all levels, ozone production efficiencies are 10–20 times higher in the upper troposphere than at the surface, and hence net chemical formation contributes almost as much O_3 as direct export at these altitudes. Most of this O_3 is lost by subsidence to the lower troposphere, where it provides almost twice as much O_3 as direct horizontal transport from the emission region. Although the lower troposphere sees greater ozone formation from advected NO_x, production efficiencies are lower, and destruction of additional O_3 transported into the region dominates. On a global scale, outside the emission region, lower tropospheric loss is greater than upper tropospheric production, and the global troposphere therefore acts as a net chemical sink of the additional pollution O_3, as indicated in Table 2.

The U.S. scenario (not shown) is qualitatively similar, and vertical and horizontal transport make similar contributions to export throughout the year; vertical transport peaks in August and leads to a maximum in additional O_3 production in the upper troposphere at this time. The European scenario shows rather different patterns, as significant wintertime titration reduces the net O_3 production, and leads to a reduction in export from the boundary layer during the period. Horizontal transport dominates removal of O_3 from the boundary layer. Vertical transport into the mid-troposphere provides little additional O_3 because of the uniformity of the vertical gradient, but sufficient NO_x is lifted by convection to contribute additional O_3 formation, peaking in spring. The proportion of iNO$_x$ tracer reaching the upper troposphere by convection is small, only 15–35% of that reaching the mid-troposphere, and the net additional O_3 production is likewise small. However, significant quantities of NO_x are exported from the region, and the upper troposphere sees net production, as for the U.S. and East Asian scenarios (see Table 2). In the boundary layer outside the region about 78% of the additional O_3 exported is deposited, compared to 56% and 55% downwind of the U.S. and East Asia. This reflects both lower net production in the emission region and greater removal downwind, where deposition over the Eurasian continent is rather faster than that over the Pacific or Atlantic Oceans. Increased production from greater horizontal transport of precursors and reduced chemical loss from competition with deposition both contribute to an increased net O_3 tendency, and in contrast to the U.S. or East Asia scenarios, there is significant additional net production outside the emission region.

4.5. Episodicity

While the main focus of this study is on monthly, regional effects, it is clear from observations [*Newell et al.,* 1996; *Jaffe et al.,* 1999; *Stohl and Trickl,* 1999] and modelling studies [*Yienger et al.,* 2000] that a significant proportion of intercontinental oxidant transport happens in a limited number of episodes when meteorological conditions are favourable. These episodes typically bring air from emission regions rather more quickly than the mean flow, and may be responsible for much of the seasonality evident in Figure 6. We investigate this by considering the temporal variations in ozone enhancements at Boulder, Hohenpeissenberg and Sapporo, from increased emissions in remote regions, see Figure 10.

Figure 1

Over each site, winter shows relatively little variability at any altitude, as vertical transport over source regions is suppressed and direct transport events are less frequent. However, lower level transport over the Atlantic is still significant, and can be seen in brief periods of enhanced North American influence over Hohenpeissenberg. The greatest variability typically occurs in the free troposphere between May and November, when greater O_3 production and more direct horizontal transport produce larger enhancements. The contrast is greatest in summer in the lower free troposphere at Boulder and Sapporo, despite less direct horizontal transport in this season, as cleaner air from more southerly latitudes removes the enhancements in 'background' O_3. Over Europe, where air mass origins are less diverse, the enhancements show less variability. In general, the impacts from upwind regions are reasonably well correlated, emphasising the similar pathways for pollutant transport; over North America, however, there is significant anti-correlation of European and Asian influences evident in the mid-troposphere in spring and autumn. While East Asian influences are driven by high level flow and subsidence, European effects are greatest at lower altitudes in more northerly flow from polar regions.

Comparison of upper tropospheric enhancements from Asian emissions over Boulder and Hohenpeissenberg reveals the propagation of a number of pollution events, most notably in May and September. In the May episode, the largest seen here, the spike in O_3 takes 8 days to reach the central U.S. and then a further 4 days to reach Europe, dropping from 2.5 to 0.67 ppbv. While the resolution of the current model may be too coarse to accurately capture the magnitude of the enhancement in this type of plume, it is clear that the model is able to capture the general behaviour of these events. However, despite the presence of distinct episodes with enhanced transport of O_3 originating in the continental boundary layer, it is clear that the variability does not dominate the mean enhancements, and that the baseline of 'background' O_3 mixing ratio experienced at these sites is substantially increased by increases in remote emissions of precursors.

4.6. Past and Future Changes

While the long-range impacts of continental emissions have been clearly detected in species such as CO, PAN and aerosols in favourable meteorological conditions [*Jaffe et al.,* 1999], the monthly-mean impacts on O_3 will be rather harder to detect due to the small size of the perturbations and the large variability in natural sources. In addition, rises in O_3 from anthropogenic sources may be partially masked by reduced influx from the lower stratosphere; *Logan et al.* [1999], analyzing trends from ozonesonde measurements between 1970 and 1996, identify a mid-latitude trend in the lower-most stratosphere of -7%/decade, but conclude that it is not yet possible to identify a general tropospheric trend in O_3.

However, *Lin et al.,* [2000], analyzing the trend in ozone at rural surface sites over the U.S. between 1980 and 1998, detect a small increase in ozone at the lower end of the probability distribution, peaking in spring, and with a secondary maximum in autumn. They suggest increases in East Asian emissions as a possible source of this, and the seasonality is very similar to what would be expected from the current study, although they find that the effects are greatest in the northeastern U.S. rather than in the northwestern U.S. as would be expected for East Asian influences. While emissions from the U.S. and Europe are thought to have changed relatively slowly over the last two decades, those from East Asia have been rising quickly. *Akimoto and Narita* [1994] estimate a factor of two increase in NO_x emissions in Asia outside Japan between 1975 and 1987, and forecasts of increases in NO_x emissions from Asia for 1990–2020 are about 4–5% per year [*van Aardenne et al.,* 1999; *Streets and Waldhoff,* 2000]. Assuming that emissions of CO and NMHCs increase proportionally, which may overestimate trends in CO emissions in particular, our results from a 10% increase in 1990 emissions suggest that an increase in mean surface ozone over the U.S. of 40–160 pptv would take 2–3 years. While this appears to account for less than half of the 3–5 ppbv increase suggested by *Lin et al.,* [2000] between 1980 and 1998, it is likely to make a substantial contribution. *Jacob et al.* [1999] suggest that a tripling of emissions over East Asia between 1985 and 2010 would lead to monthly mean surface enhancements of 2–6 pppbv over the western U.S. and 1–3 ppbv over the eastern U.S. While the non-linearity in ozone production prevents us from making a direct comparison based on 10% increased emissions, our results are in broad agreement with these conclusions, and we suggest that impacts over Europe may be only marginally smaller on an annual basis.

5. Conclusions

In this study, we have demonstrated the extent to which surface emissions of NO_x, CO and hydrocarbons from anthropogenic sources may affect oxidant concentrations in downwind regions on a hemispheric scale. Of the three Northern mid-latitudes regions considered, we find that East Asia has the greatest potential to affect tropospheric ozone, and that both North America and Europe see significant influence in surface ozone from this source, peaking in spring and autumn. However, we find the greatest intercontinental effects are over Europe due to relatively short-range transport from North American source regions. The smallest effects are seen downwind of Europe, where the continental land-mass and regional meteorology lead to lower-level outflow, greater deposition and flow to the north of the East Asian region. We suggest that Europe is the most prone as a receptor of these long-range impacts, whilst most of the East Asian region is relatively sheltered. We note that the ozone enhancements are not limited to the lower atmosphere, and that the substantial upper tropospheric enhancements, also found by *Berntsen et al.* [1996], may have important implications for climate studies, as ozone in this region has a greater radiative forcing effect than at lower altitudes in the troposphere.

The extent of these intercontinental impacts is controlled by a number of mechanisms: boundary layer production of ozone, lifting of ozone and precursors into the free troposphere, further *in-situ* chemical production, rapid and direct horizontal transport, deposition or chemical removal during transport, and eventual subsidence over receptor regions. The balance between these processes varies considerably by season and by region. While boundary layer production and convective lifting are greatest in summer, the chemical lifetime is short, and transport is less direct, poleward of the regions considered, reducing the effects in this season. The greatest impacts are seen in spring and autumn, when horizontal transport is rapid and direct, when boundary layer production and lifting are greater than in winter, but when the chemical lifetime during transport is rather greater than in summer. Although the seasonality is controlled largely by transport processes, as demonstrated with the inert $i\mathrm{NO}_x$ tracer, chemical production plays a significant role. We find that 25–40% of the total regional net production occurs above the boundary layer, and that in the upper troposphere (400–150 hPa) *in-situ* formation from transported precursors accounts for 70–85% of the O_3 from surface anthropogenic sources. Finally, we highlight the role of efficient non-convective lifting over East Asia in spring, coupled with direct horizontal transport, in enhancing the intercontinental impacts of this region.

While there is additional net O_3 production in the polluted boundary layer from increased emissions over each region, there is increased destruction in more remote parts of the lower troposphere caused by the greater export of ozone. Future increases in continental emissions are likely to increase net ozone production in those parts of the troposphere which already see net production, and to increase net destruction in sink regions such as the remote lower and mid-troposphere. This increasing polarization may become evident in greater contrasts between the chemical environment over the continents and that over the oceans, and between the upper and lower troposphere.

The emission perturbations used in the present study include only surface fossil fuel and industrial sources; no perturbation is applied to aircraft sources which may be expected to have larger impacts on upper tropospheric ozone due to direct emissions in the region. Changes in vegetation or biomass burning emissions are also not considered, although these are largely under anthropogenic control in the regions of interest. The chemical scheme used, while capturing the general features of the tropospheric distributions of the species of interest, does not account for heterogeneous chemistry on the surface of aerosols, which may lead to a reduction in boundary layer O_3 formation [*Phadnis and Carmichael*, 2000]. Future studies would benefit greatly from using appropriate meteorological data to allow more detailed testing of the conclusions with tropospheric measurements from continental margins, for example from the West coast of the U.S. Finally, this study has focussed on Northern mid-latitude effects, but increasing development in countries such as India may be expected to exert considerable influence on the oxidizing capacity of the troposphere through direct impact on tropical regions.

Acknowledgments. The authors are grateful for helpful discussions with Michael Prather, and for the useful comments of three anonymous reviewers.

References

van Aardenne, J.A., G.R. Carmichael, H. Levy, D. Streets, and L. Hordijk, Anthropogenic NO_x emissions in Asia in the period 1990–2020, *Atmos. Env., 33*, 633–646, 1999.

Akimoto, H., and H. Narita, Distribution of SO_2, NO_x and CO_2 emissions from fuel combustion and industrial activities in Asia with $1^\circ \times 1^\circ$ resolution, *Atmos. Env., 28*, 213–225, 1994.

Andreae, M.O., J. Fishman, and J. Lindesay, The Southern Tropical Atlantic Region Experiment (STARE): Transport and Atmospheric Chemistry near the Equator — Atlantic (TRACE-A) and Southern African Fire-Atmosphere Research Initiative (SAFARI): An Introduction, *J. Geophys. Res., 101*, 23,519–23,520, 1996.

Atherton, C.S., S. Sillman, and J. Walton, Three-dimensional global modeling studies of the transport and photochemistry over the North Atlantic Ocean, *J. Geophys. Res., 101*, 29,289–29,304, 1996.

Berntsen, T, I.S.A. Isaksen, W.C. Wang, and X.Z. Liang, Impacts of increased anthropogenic emissions in Asia on tropospheric ozone and climate, *Tellus, 48B*, 13–32, 1996.

Berntsen, T.K., S. Karlsdottir, and D.A. Jaffe, Influence of Asian emissions on the composition of air reaching the North Western United States, *Geophys. Res. Lett., 26*, 2171–2174, 1999.

Bethan, S, G. Vaughan, C. Gerbig, A. Volz-Thomas, H. Richer, and D.A. Tiddeman, Chemical air mass differences near fronts, *J. Geophys. Res., 103*, 13,413–13,434, 1998.

Bodhaine, B.A., J.M. Harris, J.A. Ogren, and D.J. Hofmann, Aerosol optical properties at Mauna Loa Observatory: Long-range transport from Kuwait?, *Geophys.*

Res. Lett., 19, 581–584, 1992.

Brasseur, G.P., D.A. Hauglustaine, S. Walters, P.J. Rasch, J.-F. Müller, C. Granier, and X.X. Tie, MOZART, a global chemical transport model for ozone and related chemical tracers .1. Model description, *J. Geophys. Res., 103*, 28,265–28,289, 1998.

Carver, G.D., P.D. Brown and O. Wild, The ASAD atmospheric chemistry integration package and chemical reaction database, *Computer Physics Communications, 105*, 197–215, 1997.

Chameides, W.L., and J.C.G. Walker, A photochemical theory for tropospheric ozone, *J. Geophys. Res., 78*, 8751–8760, 1973.

Chameides, W.L., P.S. Kasibhatla, J. Yienger, and H. Levy II, Growth of continental-scale metro-agro-plexes, regional ozone pollution, and world food production, *Science, 264*, 74–77, 1994.

Collins, W.J., D.S. Stevenson, C.E. Johnson, and R.G. Derwent, The European regional ozone distribution and its links with the global scale for the years 1992 and 2015, *Atmos. Env., 34*, 255–267, 2000.

Duce, R.A., C.K. Unni, B.J. Ray, J.M. Prospero, and J.T. Merrill, Long-range atmospheric transport of soil dust from Asia to the tropical North Pacific, *Science, 209*, 1522–1524, 1980.

Fehsenfeld, F.C., P. Daum, W.R. Leaitch, M. Trainer, D.D. Parrish, and G. Hübler, Transport and processing of O_3 and O_3 precursors over the North Atlantic: An overview of the 1993 North Atlantic Regional Experiment (NARE) summer intensive, *J. Geophys. Res., 101*, 28,877–28,891, 1996.

Guenther, A., C.N. Hewitt, D. Erikson, R. Fall, C. Geron, et al., A global model of natural volatile organic compound emissions, *J. Geophys. Res., 100*, 8873–9992, 1995.

Hoell, J.M., D.D. Davis, S.C. Liu, R.E. Newell, H. Akimoto, R.J. McNeal, and R.J. Bendura, The Pacific Exploratory Mission-West Phase B: February-March 1994, *J. Geophys. Res., 102*, 28,223–28,240, 1997.

Horowitz, L.W., J.Y. Liang, G.M. Gardner, and D.J. Jacob, Export of reactive nitrogen from North America during summertime: Sensitivity to hydrocarbon chemistry, *J. Geophys. Res., 103*, 13,451–13,476, 1998.

Jacob, D.J., S.M. Fan, S.C. Wofsy, P.A. Spiro, P.S. Bakwin, J.A. Witter, E.V. Browell, G.L. Gregory, D.R. Fitzjarrald, and K.E. Moore, Deposition of ozone to tundra, *J. Geophys. Res., 97*, 16,473–16,479, 1992.

Jacob, D.J., J.A. Logan, G.M. Gardner, R.M. Yevich, C.M. Spivakovsky, and S.C. Wofsy, Factors regulating ozone over the United States and its export to the global atmosphere, *J. Geophys. Res., 98*, 14,817–14,826, 1993.

Jacob, D.J., J.A. Logan, and P.P. Murti, Effect of rising Asian emissions on surface ozone in the United States, *Geophys. Res. Lett., 26*, 2175–2178, 1999.

Jaffe, D., et al., Transport of Asian air pollution to North America, *Geophys. Res. Lett., 26*, 711–714, 1999.

Kotamarthi, V.R., and G.R. Carmichael, The long range transport of pollutants in the Pacific Rim region, *Atmos. Env., 24*, 1521–1534, 1990.

Liang., J.Y., and M.Z. Jacobson, Effects of subgrid segregation on ozone production efficiency in a chemical model, *Atmos. Env., 34*, 2975–2982, 2000.

Liang., J.Y., L.W. Horowitz, D.J. Jacob, Y. Wang, A.M. Fiore, J.A. Logan, G.M. Gardner, and J.W. Munger, Seasonal budgets of reactive nitrogen species and ozone over the United States, and export fluxes to the global atmosphere, *J. Geophys. Res., 103*, 13,435–13,450, 1998.

Lin, C.-Y., D.J. Jacob, J.W. Munger, and A.M. Fiore, Increasing background ozone in surface air over the United States, *Geophys. Res. Lett., 27*, 3465-3468, 2000.

Lin, X., M. Trainer, and S.C. Liu, On the non-linearity of tropospheric ozone production, *J. Geophys. Res., 93*, 15,879–15,888, 1988.

Logan, J.A., An analysis of ozonesonde data for the troposphere: Recommendations for testing 3-D models, and development of a gridded climatology for tropospheric ozone, *J. Geophys. Res., 104*, 16,115–16,149, 1999.

Logan, J.A., I.A. Megretskaia, A.J. Miller, G.C. Tiao, D. Choi, L. Zhang, L. Bishop, R. Stolarski, G.J. Labow, S.M. Hollandsworth, G.E. Bodeker, H. Claude, D. DeMuer, J.B. Kerr, D.W. Tarasick, S.J. Oltmans, B. Johnson, F. Schmidlin, J. Staehelin, P. Viatte, and O. Uchino, Trends in the vertical distribution of ozone: a comparison of two analyses of ozonesonde data, *J. Geophys. Res., 104*, 26,373–26,399, 1999.

Louis, J.F., A parametric model of vertical eddy fluxes in the atmosphere, *Boundary Layer Meteorology, 17*, 187–202, 1979.

Mauzerall, D.L., D. Narita, H. Akimoto, L. Horowitz, S. Waters, D.A. Hauglustaine, and G. Brasseur, Seasonal characteristics of tropospheric ozone production and mixing ratios over East Asia: A global three-dimensional chemical transport model analysis, *J. Geophys. Res., 105*, 17,895–17,910, 2000.

McLinden, C.A., S. Olsen, B. Hannegan, O. Wild, M.J. Prather, and J. Sundet, Stratospheric ozone in 3-D models: A simple chemistry and the cross-tropopause flux, *J. Geophys. Res., 105*, 14,653–14,665, 2000.

Monks, P.S., A review of the observations and origins of the spring ozone maximum, *Atmos. Environ., 34*, 3545–3561, 2000.

Newell, R.E., et al., Vertical fine-scale atmospheric structure measured from NASA DC-8 during PEM-West A, *J. Geophys. Res., 101*, 1943–1960, 1996.

Olivier, J.G.J., et al., Description of EDGAR Version 2.0, RIVM/TNO report 771060 002, RIVM, Bilthoven, December 1996.

Phadnis, M.J., and G.R. Carmichael, Numerical investigation of the influence of mineral dust on the tropospheric

chemistry of East Asia, *J. Atmos. Chem., 36*, 285–323, 2000.

Pickering, K.E., A.M. Thompson, R.R. Dickerson, W.T. Luke, D.P. McNamara, J.P. Greenberg, and P.R. Zimmerman, Model-calculations of tropospheric ozone production potential following observed convective events, *J. Geophys. Res., 95*, 14,049–14,062, 1990.

Prather, M. J., Numerical advection by conservation of second-order moments, *J. Geophys. Res., 91*, 6671–6681, 1986.

Price, C., and D. Rind, A simple lightning parameterization for calculating global lightning distributions, *J. Geophys. Res., 97*, 9919–9933, 1992.

Rind, D., J. Lerner, K. Shah, and R. Suozzo, Use of online tracers as a diagnostic tool in general circulation model development, 2, Transport between the troposphere and stratosphere, *J. Geophys. Res., 104*, 9151–9167, 1999.

Stohl, A., and T. Trickl, A textbook example of long-range transport: Simultaneous observation of ozone maxima of stratospheric and North American origin in the free troposphere over Europe, *J. Geophys. Res., 104*, 30,445–30,462, 1999.

Streets, D.G., and S.T. Waldhoff, Present and future emissions of air pollutants in China: SO2, NO_x, and CO, *Atmos. Env., 34*, 363–374, 2000.

Volz, A., and D. Kley, Evaluation of the Montsouris series of ozone measurements made in the nineteenth century, *Nature, 322*, 240–242, 1988.

Wild, O., and M.J. Prather, Excitation of the primary tropospheric chemical mode in a global 3-D model, *J. Geophys. Res., 105*, 24,647–24,660, 2000.

Wild, O., X. Zhu and M.J. Prather, Fast-J: Accurate simulation of in- and below-cloud photolysis in tropospheric chemical models, *J. Atmos. Chem., 37*, 245–282, 2000.

Yienger, J.J., and H. Levy II, Empirical model of global soil-biogenic NO_x emissions, *J. Geophys. Res., 100*, 11,447–11,464, 1995.

Yienger, J.J., M.K. Galanter, T.A. Holloway, M.J. Phadnis, S.K. Guttikunda, G.R. Carmichael, W.J. Moxim, and H. Levy II, The episodic nature of air pollution transport from Asia to North America, *J. Geophys. Res., 105*, 26,931–26,945, 2000.

H. Akimoto and O. Wild, Frontier Research System for Global Change, 3173-25 Showa-machi, Kanazawa-ku, Yokohama, Kanagawa 236-0001, Japan. (email: oliver@frontier.esto.or.jp)

Received October 31, 2000

Figure 1. Monthly-mean O_3 mixing ratios over Boulder (40°N, 105°W), Hohenpeissenberg (48°N, 11°E) and Sapporo (43°N, 141°E) in the lower, mid- and upper troposphere; model means (dashed lines) and mulit-year mean ozonesonde measurements (solid lines) [*Logan*, 1999].

Figure 2. Components of the tropospheric ozone budget in the FRSGC/UCI CTM by hemisphere, showing the contribution of net influx from the stratosphere (top), net chemical tendency (middle), and deposition at the surface (bottom) in each hemisphere, month-by-month. Net tendencies are given in Tg/month.

Figure 3. The annual distribution of NO_x emissions from industrial/fossil fuel sources (in kgN/yr) from EDGAR v2.0 [*Olivier et al.*, 1996] on a $4° \times 5°$ grid. The regions used in the current study are highlighted; Japan has been included in the East Asian region for defining total exports (Table 1), but is not included in the perturbation studies to allow a more realistic assessment of the effects of rapid development of other countries in the region.

Figure 4. Annual zonal, column and meridional mean differences in O_3 mixing ratios (in pptv) due to 10% increased emissions over East Asia (top row), the U.S. (middle row), and Europe (bottom row).

Figure 5. Annual zonal, column and meridional mean differences in net chemical O_3 tendencies (in $ng/m^2/s$) due to 10% increased emissions over East Asia, the U.S., and Europe.

Figure 6. Differences in monthly mean O_3 mixing ratios (in ppbv) at the surface, 650 hPa and 200 hPa over East Asia, the U.S., and Europe (columns) for 10% increased emissions in each region (rows). Shaded plots indicate the region with increased emissions; error bars indicate the spatial variance of monthly means within each region.

Figure 7. Differences in monthly mean $i\mathrm{NO}_x$ mixing ratios (in ppbv) at the surface, 650 hPa and 200 hPa over East Asia, the U.S., and Europe (columns) for 10% increased emissions in each region (rows). Shaded plots indicate the region with increased emissions; error bars indicate the spatial variance of monthly means within each region.

Figure 8. Monthly mass fluxes of O_3 (in Tg/month) through the physical processes controlling removal or export of pollution ozone from the continental boundary layer for the additional O_3 formed from 10% increased fossil fuel emissions in each region.

Figure 9. Differences in the mass flux (in Tg/month) through different processes for (left) the decaying $i\mathrm{NO}_x$ tracer and (right) O_3 caused by 10% increased emissions over East Asia. Positive values indicate formation or import, negative values destruction or export; note that the terms are additive, and hence that the six domains cover the global troposphere from the surface to 150 hPa.

Figure 10. Enhancements in three-hourly O_3 mixing ratios over Boulder (40°N, 105°W), Hohenpeissenberg (48°N, 11°E) and Sapporo (43°N, 141°E) in the lower, mid- and upper troposphere; for comparison with the monthly means at these sites, see Figure 1.

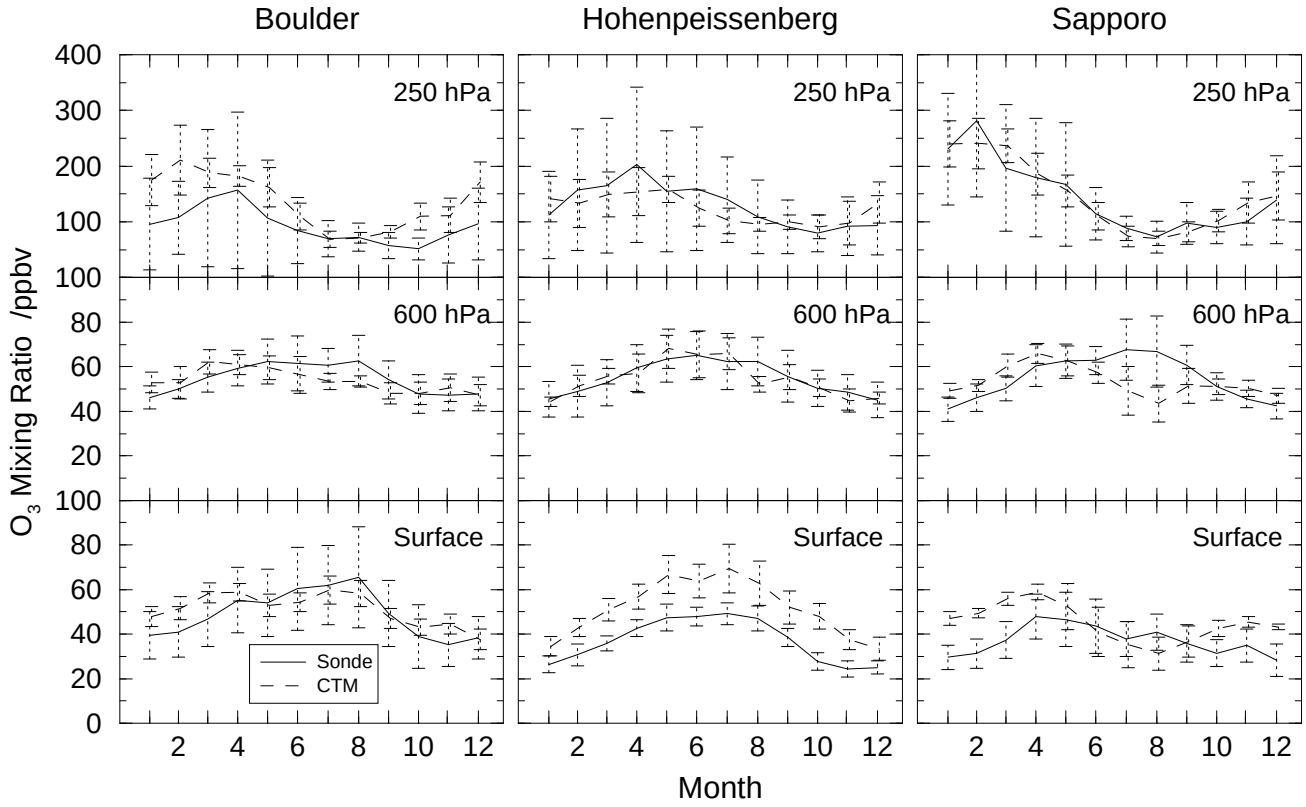

Figure 1. Monthly-mean O_3 mixing ratios over Boulder (40°N, 105°W), Hohenpeissenberg (48°N, 11°E) and Sapporo (43°N, 141°E) in the lower, mid- and upper troposphere; model means (dashed lines) and multi-year mean ozonesonde measurements (solid lines) [*Logan*, 1999].

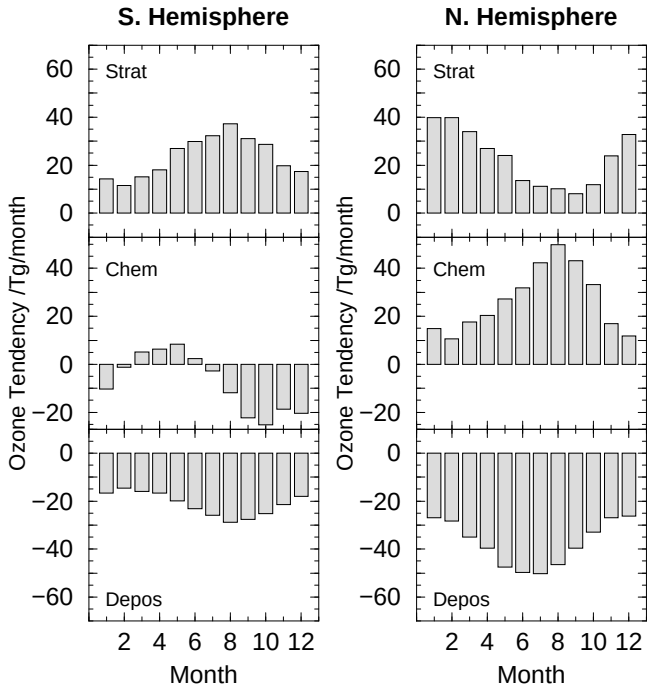

Figure 2. Components of the tropospheric ozone budget in the FRSGC/UCI CTM by hemisphere, showing the contribution of net influx from the stratosphere (top), net chemical tendency (middle), and deposition at the surface (bottom) in each hemisphere, month-by-month. Net tendencies are given in Tg/month.

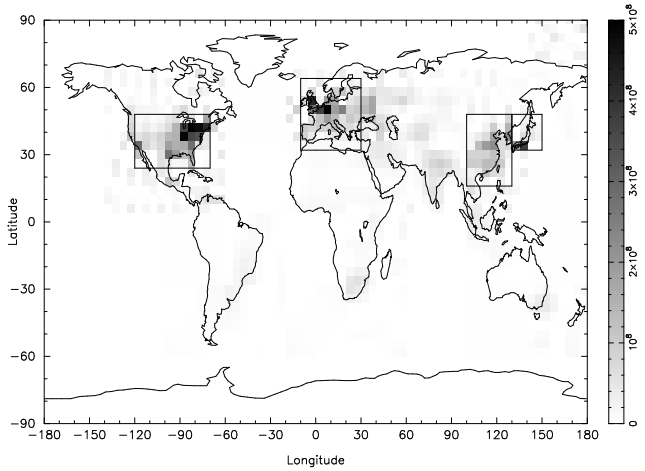

Figure 3. The annual distribution of NO_x emissions from industrial/fossil fuel sources (in kgN/yr) from EDGAR v2.0 [*Olivier et al.*, 1996] on a 4°× 5° grid. The regions used in the current study are highlighted; Japan has been included in the East Asian region for defining total exports (Table 1), but is not included in the perturbation studies to allow a more realistic assessment of the effects of rapid development of other countries in the region.

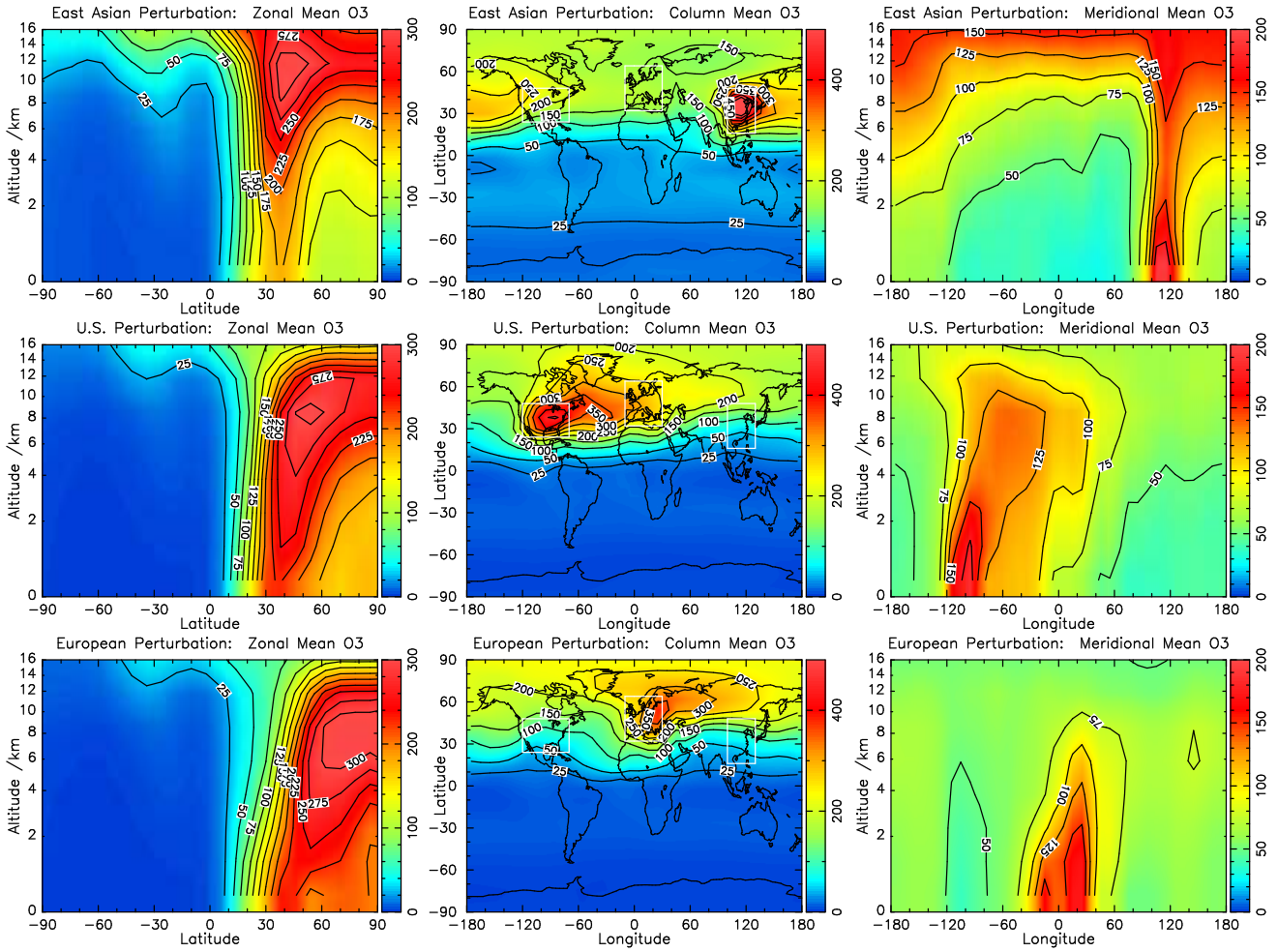

Figure 4. Annual zonal, column and meridional mean differences in O_3 mixing ratios (in pptv) due to 10% increased emissions over East Asia (top row), the U.S. (middle row), and Europe (bottom row).

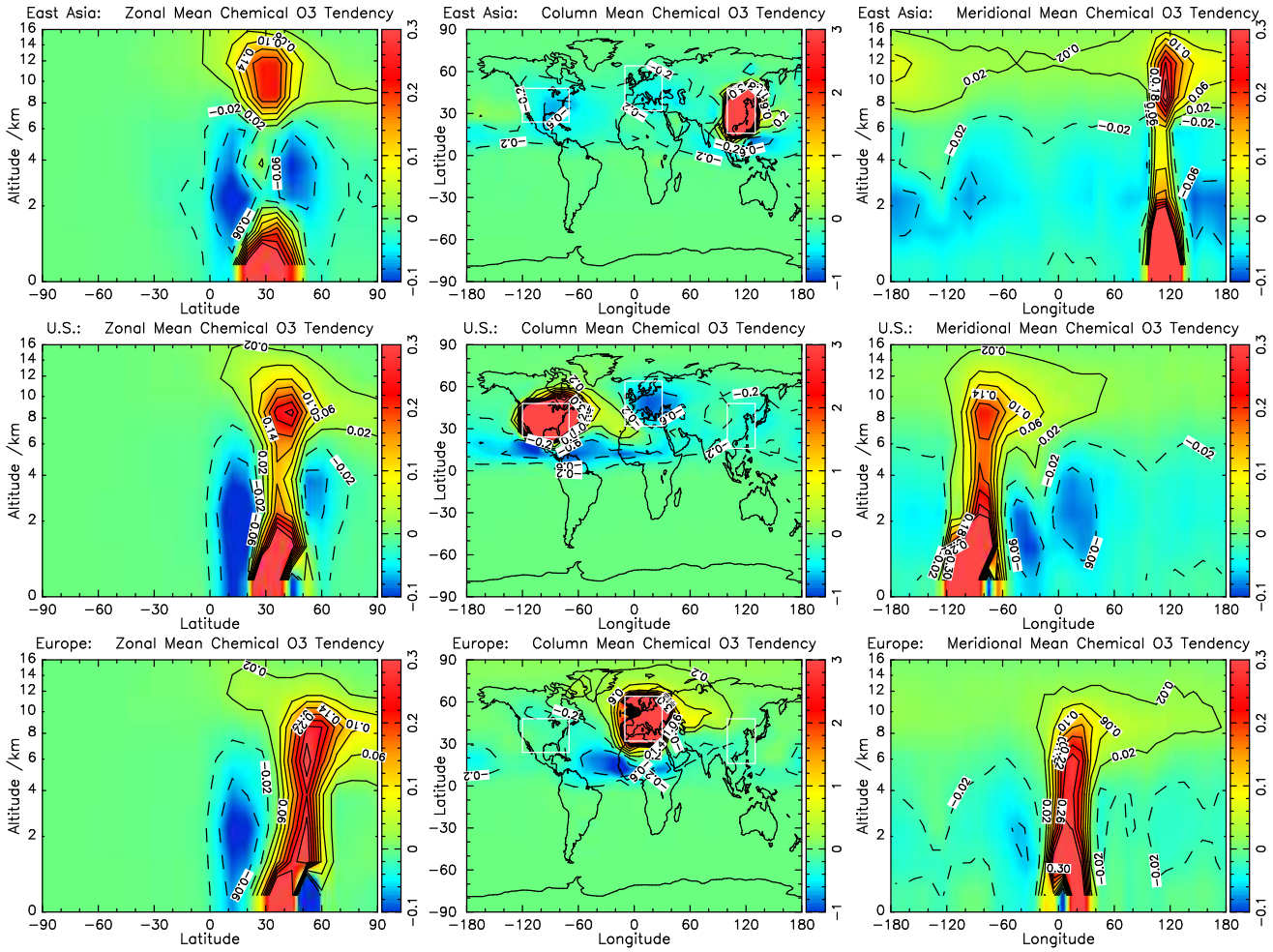

Figure 5. Annual zonal, column and meridional mean differences in net chemical O_3 tendencies (in ng/m^2/s) due to 10% increased emissions over East Asia, the U.S., and Europe.

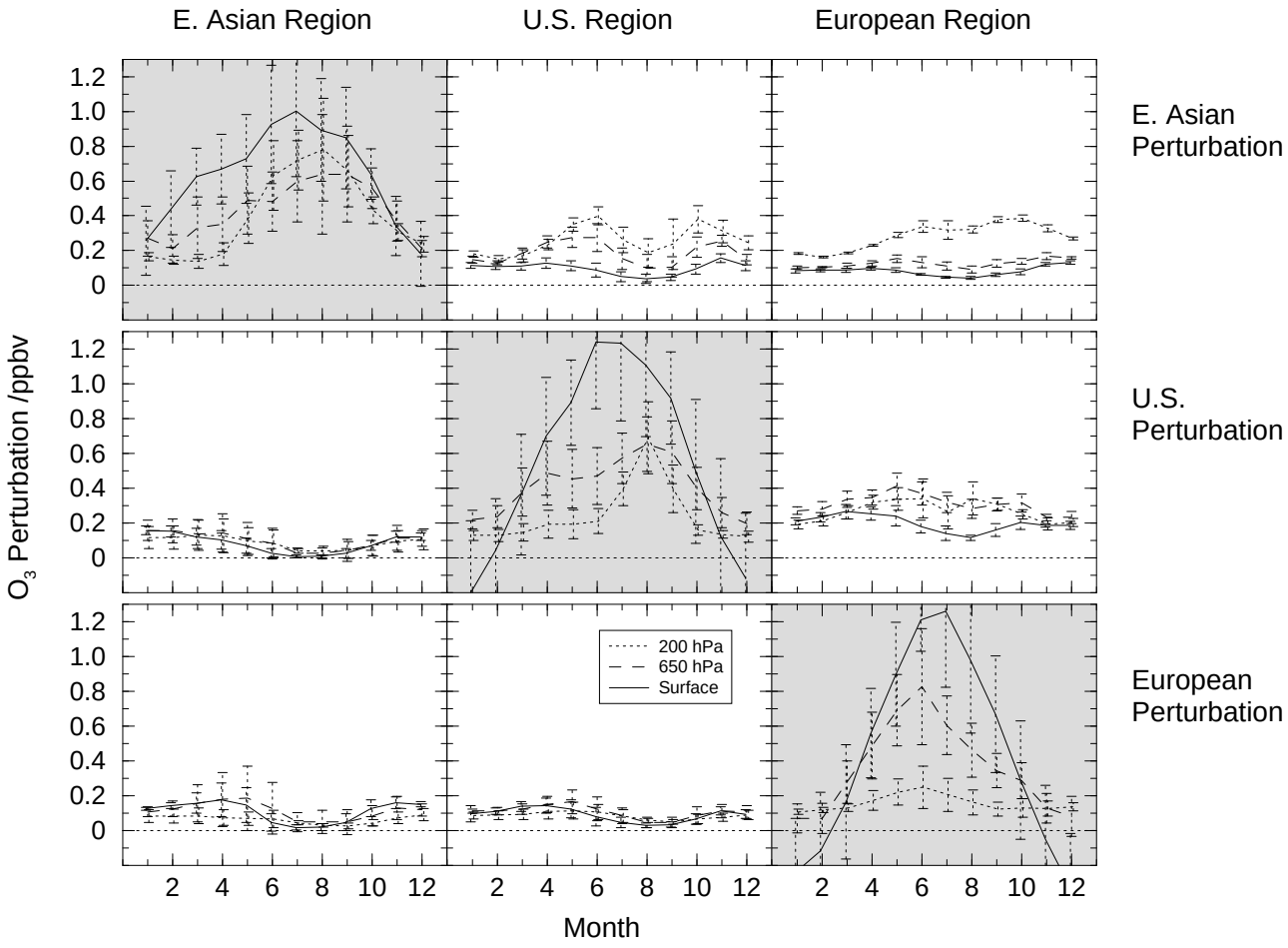

Figure 6. Differences in monthly mean O_3 mixing ratios (in ppbv) at the surface, 650 hPa and 200 hPa over East Asia, the U.S., and Europe (columns) for 10% increased emissions in each region (rows). Shaded plots indicate the region with increased emissions; error bars indicate the spatial variance of monthly means within each region.

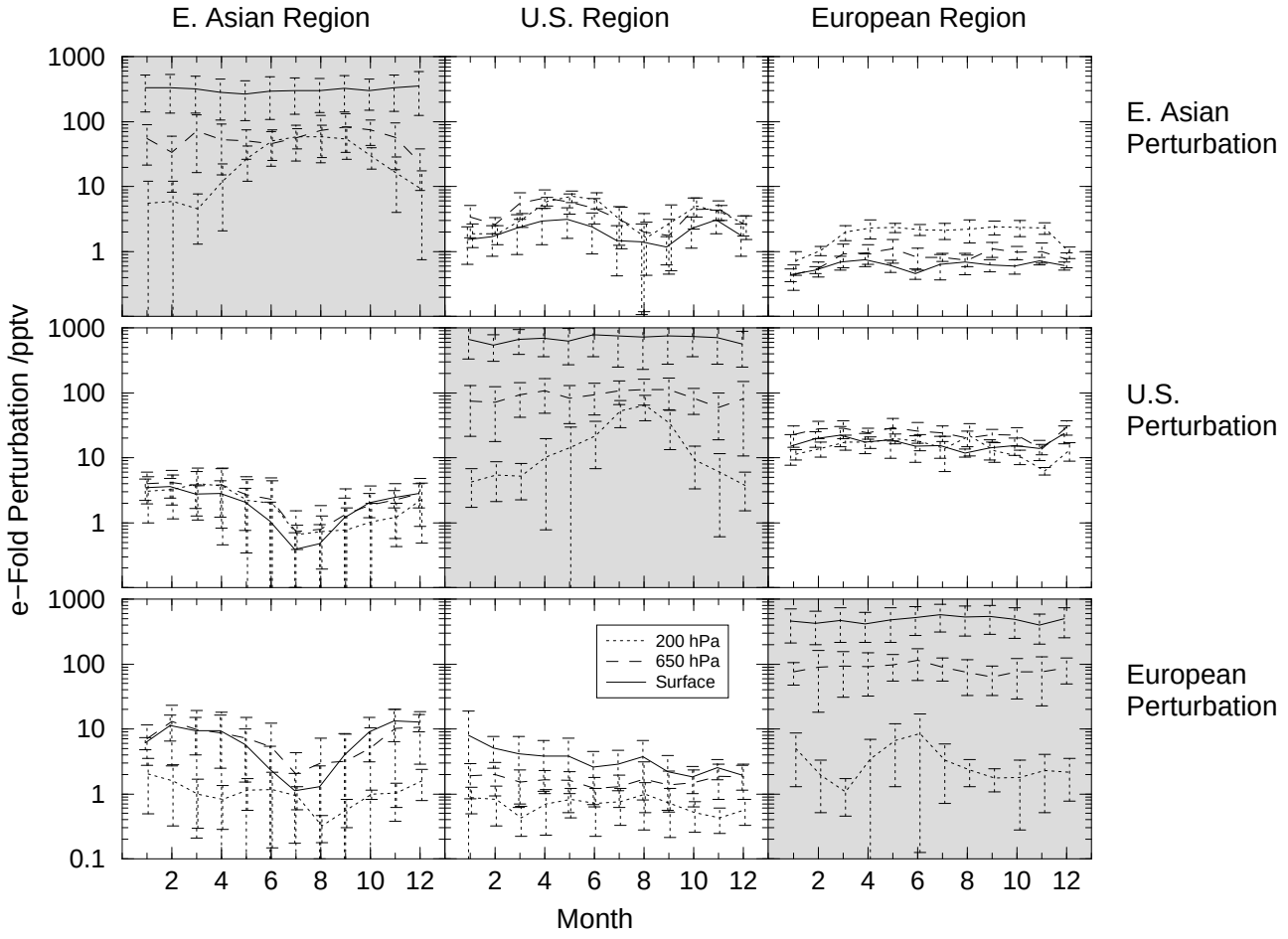

Figure 7. Differences in monthly mean $i\mathrm{NO}_x$ mixing ratios (in ppbv) at the surface, 650 hPa and 200 hPa over East Asia, the U.S., and Europe (columns) for 10% increased emissions in each region (rows). Shaded plots indicate the region with increased emissions; error bars indicate the spatial variance of monthly means within each region.

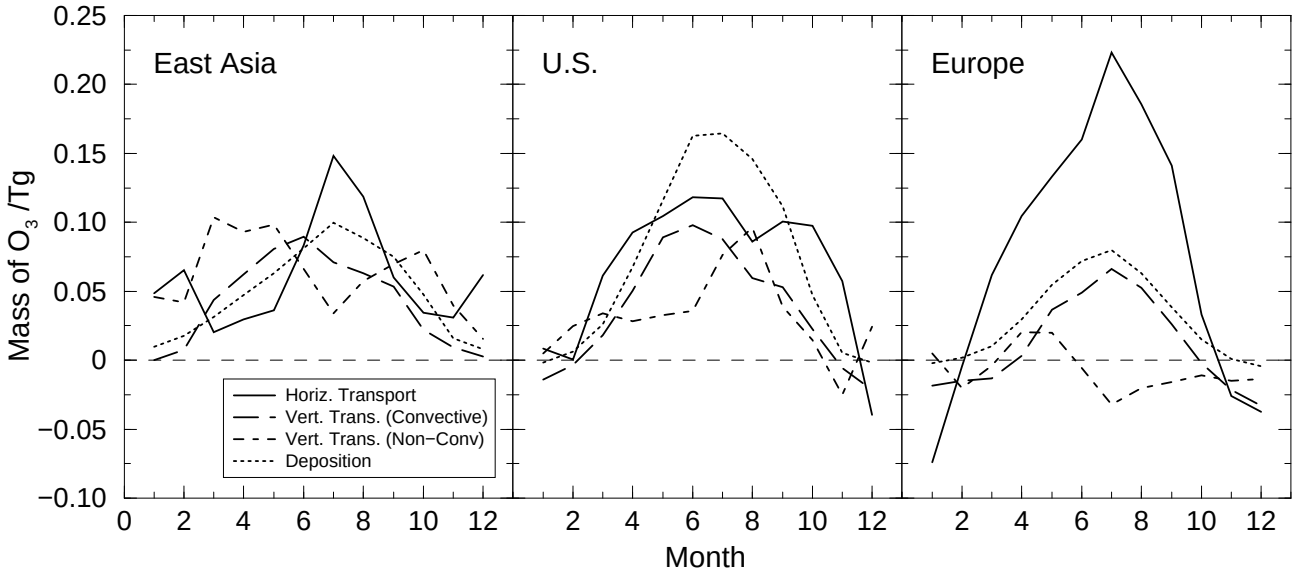

Figure 8. Monthly mass fluxes of O_3 (in Tg/month) through the physical processes controlling removal or export of pollution ozone from the continental boundary layer for the additional O_3 formed from 10% increased fossil fuel emissions in each region.

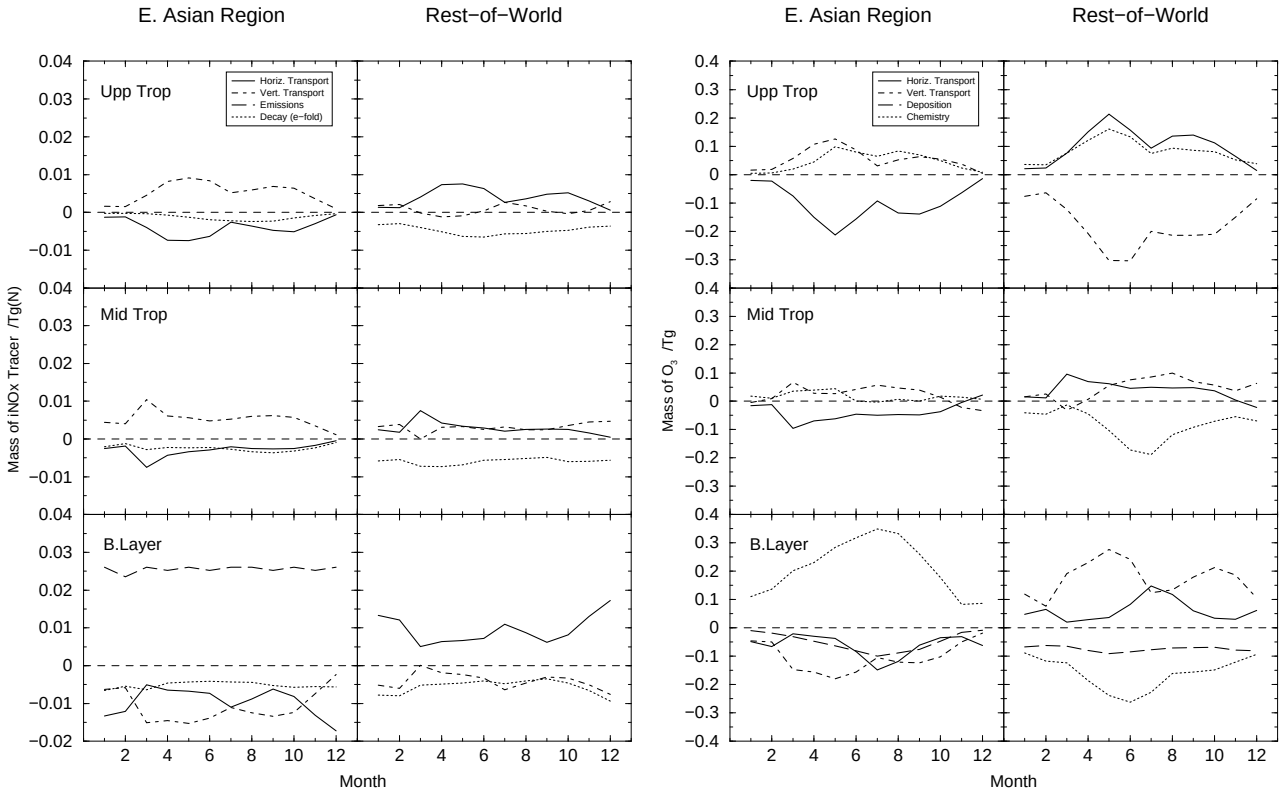

Figure 9. Differences in the mass flux (in Tg/month) through different processes for (left) the decaying $i\mathrm{NO}_x$ tracer and (right) O_3 caused by 10% increased emissions over East Asia. Positive values indicate formation or import, negative values destruction or export; note that the terms are additive, and hence that the six domains cover the global troposphere from the surface to 150 hPa.

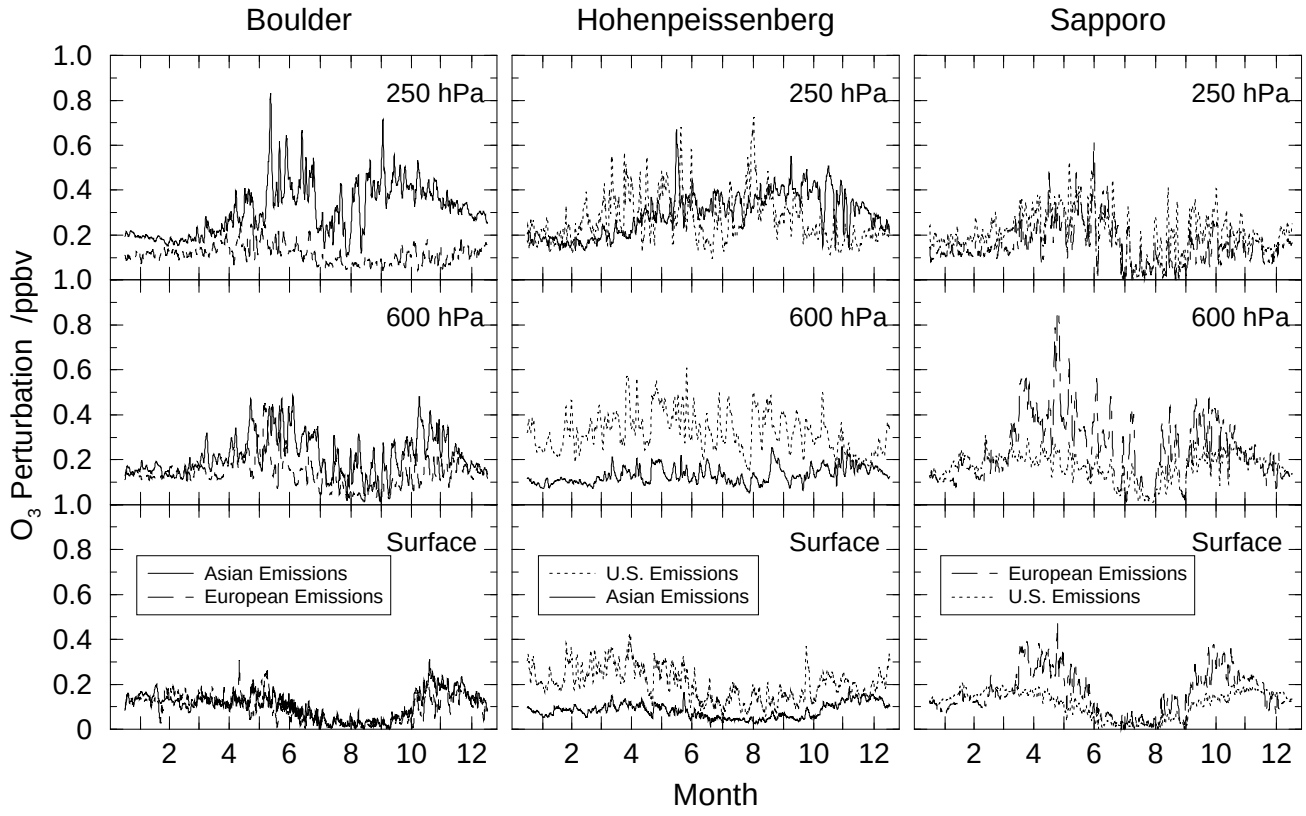

Figure 10. Enhancements in three-hourly O_3 mixing ratios over Boulder (40°N, 105°W), Hohenpeissenberg (48°N, 11°E) and Sapporo (43°N, 141°E) in the lower, mid- and upper troposphere; for comparison with the monthly means at these sites, see Figure 1.

Table 1. Annual Regional O_3 and NO_x Budgets

	U. States	Europe	E. Asia
Regional Boundary Layer O_3 (Tg/yr)			
Net O_3 production	60.5	30.7	49.1
O_3 deposition	49.1	27.2	34.5
Net O_3 export	11.4	3.4	14.7
O_3 prod. efficiency	3.10	2.25	3.90
Summer (JJA)	4.80	3.84	6.41
Winter (DJF)	1.10	0.05	2.21
Regional Boundary Layer NO_x (Tg(N)/yr)			
NO_x emissions	7.68	5.79	4.67
NO_x+PAN export	1.41	1.24	1.14
Fraction exported	18%	21%	24%
Total Regional O_3 up to 150 hPa (Tg/yr)			
Net O_3 production	81.5	49.1	74.7
Net O_3 export	32.3	21.9	40.2
Strat O3 import	19.3	14.3	13.2
Trop O3 export	51.6	36.2	53.4

Table 2. Production and Fate of Anthropogenic O_3 From 10% Increased Emissions in Each Region

	U. States	Europe	E. Asia
Global Tropospheric O_3 (Tg/yr)			
Net O_3 production	2.13	2.00	1.65
O_3 deposition	2.04	1.91	1.48
Regional Boundary Layer O_3 (Tg/yr)			
Net O_3 production	2.48	1.30	2.57
O_3 deposition	0.85	0.36	0.58
Net O_3 export	1.63	0.94	1.99
Fraction exported	66%	72%	77%
O_3 prod. efficiency	1.24	0.92	2.74
Upper Tropospheric O_3, 400–150 hPa (Tg/yr)			
O_3 prod. (regional)	0.32	0.20	0.55
(global)	1.20	0.88	1.53
Vertical transport	0.46	0.14	0.65
contrib.	28%	14%	30%